Surface & Coatings Technology 442 (2022) 128273

Contents lists available at ScienceDirect

Surface & Coatings Technology

journal homepage: www.elsevier.com/locate/surfcoat

Transfer of the sputter technique for deposition of strongly thermochromic VO_2-based coatings on ultrathin flexible glass to large-scale roll-to-roll device

Jiří Rezek [a], Jolanta Szelwicka [b], Jaroslav Vlček [a,*], Radomír Čerstvý [a], Jiří Houška [a], Matthias Fahland [b], John Fahlteich [b]

[a] Department of Physics and NTIS – European Centre of Excellence, University of West Bohemia, Univerzitní 8, 306 14 Plzeň, Czech Republic
[b] Fraunhofer Institute for Organic Electronics, Electron Beam and Plasma Technology FEP, Winterbergstrasse 28, 01277 Dresden, Germany

ARTICLE INFO

Keywords:
Vanadium dioxide
Strongly thermochromic coatings
Roll-to-roll device
Pulsed magnetron sputtering
Ultrathin flexible glass
Smart windows

ABSTRACT

The reversible semiconductor-to-metal transition of vanadium dioxide (VO_2) makes VO_2-based coatings a promising candidate for thermochromic smart windows, reducing the energy consumption of buildings. We report on transfer of the sputter technique for deposition of strongly thermochromic ZrO_2/W-doped VO_2/ZrO_2 coatings on ultrathin (0.1 mm) flexible glass from a laboratory-scale device with three (V, W and Zr) planar magnetron targets to a large-scale roll-to-roll device with two (W-doped V and ZrO_2) rotatable magnetron targets. The depositions were performed at a relatively low substrate surface temperature (330–350 °C) and without any substrate bias voltage. The W-doped VO_2 layers were deposited using a reactive high-power impulse magnetron sputtering with a pulsed O_2 flow control. We compare the process parameters used in both deposition devices and explain the basic principle of this sputter technique using the discharge characteristics measured during a large-scale roll-to-roll deposition. We characterize the design, structure (X-ray diffraction) and optical properties (spectrophotometry and spectroscopic ellipsometry) of the three-layer coatings. The coatings prepared on ultrathin flexible glass using the large-scale roll-to-roll device at a temperature close to 350 °C exhibit a low transition temperature of 22 °C, an integral luminous transmittance over 45% and a modulation of the solar energy transmittance approaching 10%. This is a promising first step to a cost-effective and high-rate preparation of large-area thermochromic VO_2-based coatings for future smart-window applications.

1. Introduction

Vanadium dioxide (VO_2) exhibits a reversible phase transition from a low-temperature monoclinic VO_2(M1) semiconducting phase to a high-temperature tetragonal VO_2(R) metallic phase at a transition temperature (T_{tr}) of approximately 68 °C for the bulk material [1,2]. This structure transition is accompanied by significant changes in the infrared transmittance, and in electrical and thermal conductivity, which make VO_2-based films a suitable candidate for numerous applications, such as electronic devices, thermal sensors and energy-saving smart windows with automatically varying solar energy transmission [3–5].

There have been many investigations and much progress in thermochromic VO_2-based materials in recent years (see, for example, reviews [6–11] and the works cited therein). However, there are still obstacles impeding their applications to smart windows. To meet the requirements for large-scale implementation on building glass, VO_2-based coatings should satisfy the following strict criteria simultaneously (see [12] and the works cited therein): a deposition temperature close to 300 °C or lower, T_{tr} close to 20 °C, a luminous transmittance $T_{lum} > 60\%$, a modulation of the solar energy transmittance $\Delta T_{sol} > 10\%$, long-time environmental stability, and a more appealing color than usual yellowish or brownish colors in transmission (smart window as seen from the inside). Moreover, a cost-effective technique for fast deposition of large-area thermochromic VO_2-based coatings for future smart-window applications should be developed.

Magnetron sputter deposition with its versatility and the potential of scaling up to large substrate sizes, is arguably the most important preparation technique of thermochromic VO_2-based coatings [11,13,14].

* Corresponding author.
E-mail address: vlcek@kfy.zcu.cz (J. Vlček).

https://doi.org/10.1016/j.surfcoat.2022.128273

Available online 24 February 2022

In our recent paper [12], we reported on high-performance three-layer thermochromic $ZrO_2/V_{0.982}W_{0.018}O_2/ZrO_2$ coatings prepared on soda-lime glass using a pulsed magnetron sputtering at a relatively low substrate surface temperature $T_s = 330$ °C and without any substrate bias voltage. The thermochromic $V_{0.982}W_{0.018}O_2$ layers were deposited by a controlled high-power impulse magnetron sputtering (HiPIMS) of a V target, combined with a simultaneous pulsed dc magnetron sputtering of a W target to reduce the transition temperature to $T_{tr} = 20$–21 °C, in an argon-oxygen gas mixture. The $ZrO_2/V_{0.982}W_{0.018}O_2/ZrO_2$ coatings exhibited T_{lum} up to 50% at ΔT_{sol} above 10% for a $V_{0.982}W_{0.018}O_2$ layer thickness of 69 nm. Let us recall that the first low-temperature deposition of thermochromic VO_2 films using HiPIMS, but with a substrate bias voltage, was presented in [15].

Our preceding paper [16] dealt with the optimization of the deposition technique for preparation of three-layer thermochromic $ZrO_2/V_{1-x}W_xO_2/ZrO_2$ coatings on ultrathin flexible glass (UFG) and standard glass in large-scale deposition systems. A high maximum target power density (spatially averaged over the total target area) in a pulse during the HiPIMS of the V target [12] was decreased three times to 1.4 kWcm^{-2} at almost the same deposition-averaged target power density of 13.5 Wcm^{-2}. To avoid atmospheric contamination and to reduce the total deposition time, the preparation of the $ZrO_2/V_{0.984}W_{0.016}O_2/ZrO_2$ coatings was performed in the same vacuum chamber without venting it to the atmosphere between the depositions of individual layers.

In the present paper, we report on transfer of this sputter technique for deposition of strongly thermochromic ZrO_2/W-doped VO_2/ZrO_2 coatings on ultrathin (0.1 mm) flexible glass from the laboratory-scale device with three (V, W and Zr) planar magnetron targets [16] at the University of West Bohemia (UWB) to a large-scale roll-to-roll device with two (W-doped V and ZrO_2) rotatable magnetron targets at the Fraunhofer Institute for Organic Electronics, Electron Beam and Plasma Technology FEP (FEP). The UFG was introduced to the market recently [17] as an alternative both to thick (rigid) glass sheets and to flexible polymer substrates. Its material properties are similar to those of rigid glass, but the thickness is much lower, ranging from 0.2 mm down to 0.02 mm [18]. In contrast to most polymers, the UFG is stable at much higher temperatures (even above 500 °C). Therefore, it can be used as a substrate for deposition of thermochromic VO_2-based coatings. Bendability of the UFG enables its high-volume processing using a roll-to-roll deposition device with magnetron sputter sources [17–19]. Because of the low weight of the UFG, this opens up the possibility for new smart-window applications of thermochromic VO_2-based coatings, such as retrofitting of existing low-efficiency glass windows [20] and the manufacturing of new high-efficiency insulated glass units with multiple functionalities (for example, a combination with electrochromic coatings).

2. Experimental details

2.1. Coating preparation

The basic characteristics of both devices used for depositions of ZrO_2/W-doped VO_2/ZrO_2 coatings on 0.1 mm thick flexible glass (Nippon Electric Glass Co., Ltd.) substrate without any substrate bias voltage in argon-oxygen gas mixtures are given in Table 1.

2.1.1. Laboratory-scale device

The $ZrO_2/V_{0.984}W_{0.016}O_2/ZrO_2$ coating was prepared at the UWB in an ultra-high vacuum multi-magnetron sputter device (ATC 2200-V AJA International Inc.) equipped by three unbalanced magnetrons with planar V, W and Zr targets at the argon partial pressure $p_{ar} = 1$ Pa. The values of p_{ar} and of $p_{tot} = p_{ar} + p_{ox}$, where p_{ox} is the oxygen partial pressure in the chamber, were measured at the chamber wall using a high-stability capacitance manometer (Baratron, Type 127, MKS) with an accuracy much better than 1%.

The $V_{0.984}W_{0.016}O_2$ layer was deposited by controlled HiPIMS of a V target, combined with a simultaneous pulsed dc magnetron sputtering of a W target, at the substrate surface temperature $T_s = 330$ °C. The argon flow rate was 60 sccm corresponding to $p_{ar} = 1$ Pa, while the total oxygen flow rate, Φ_{ox}, in two to-substrate O_2 inlets, injecting oxygen in front of the V sputtered target, was not fixed but alternating between 1.45 sccm and 1.85 sccm (see Table 2). The moments of switching of the Φ_{ox} pulses from one value to the other were determined during the deposition by a programmable logic controller using a pre-selected critical value of the discharge current on the V target. This simple process control, explained in [16], makes it possible to deliver a high power into discharge pulses without arcing on the V target surface and thus, to utilize exclusive benefits of the HiPIMS discharges in the preparation of crystalline thermochromic VO_2-based layers on unbiased non-conductive substrates at relatively low T_s [21,22]. The magnetron with the V target was driven by a unipolar high-power pulsed dc power supply (TruPlasma Highpulse 4002, TRUMPF Huettinger). The voltage pulse duration was 80 μs at a repetition frequency of 625 Hz (duty cycle of 5%) and the deposition-averaged target power density was 13.5 Wcm^{-2}. The magnetron with the W target was driven by a unipolar pulsed dc power supply (IAP-1010 EN Technologies Inc.). The voltage pulse duration was 16 μs at a repetition frequency of 5 kHz (duty cycle of 8%) and the deposition-averaged target power density was 35 mWcm^{-2}.

Both the bottom and the top ZrO_2 layer were deposited by reactive pulsed dc magnetron sputtering onto substrates without any external heating ($T_s < 60$ °C). The oxygen partial pressure was 0.12 Pa (oxide mode) at $\Phi_{ox} = 9$ sccm. The magnetron with the Zr target was driven by an asymmetric bipolar pulsed dc power supply (TruPlasma Bipolar 4010, TRUMPF Huettinger). The negative-voltage pulse duration was 6.25 μs at a repetition frequency of 80 kHz (duty cycle of 50%) and the average target power density was 12.6 Wcm^{-2} in these negative pulses. Further details on the deposition process can be found in [16].

2.1.2. Large-scale roll-to roll device

The ZrO_2/W-doped VO_2/ZrO_2 coatings were prepared at the FEP in a large-scale roll-to-roll device (FOSA LabX 330 Glass, Von Ardenne GmbH) equipped by two magnetrons with W-doped (1.5 at.%, resulting in almost the same x characterizing the $V_{1-x}W_xO_2$ layer deposited on the used roll substrate) V, denoted as V-W from now on, and ZrO_2 rotatable (15 rpm) targets in two individual sputter chambers (see Fig. 1 and Table 1). Dual-anode magnetron configurations [23] were used to

Table 1
Basic characteristics of the laboratory-scale device and the large-scale roll-to-roll device used for depositions of ZrO_2/W-doped VO_2/ZrO_2 coatings at the University of West Bohemia (UWB) and at the Fraunhofer FEP (FEP), respectively. Here, d and l is the diameter and length, respectively.

	Laboratory device (UWB)	Roll-to-roll device (FEP)
Vacuum chamber	$d = 560$ mm, $l = 430$ mm	$d = 2760$ mm, $l = 1170$ mm
Targets	Planar V, W and Zr ($d = 50$ mm in all cases)	Rotatable W-doped (1.5 at.%) V ($d = 139$ mm, $l = 665$ mm) and ZrO_2 ($d = 139$ mm, $l = 679$ mm)
Substrate	Fixed sheeth (25 × 50 mm^2) on rotating (20 rmp) holder	Moving roll (300 × 20 000 mm^2)
Target-to-substrate distance	145 mm	80 mm

Table 2
Process parameters during the depositions of the thermochromic $V_{0.984}W_{0.016}O_2$ layer using a controlled high-power impulse magnetron sputtering (HiPIMS) of a V target, combined with a simultaneous pulsed dc magnetron sputtering of a W target, at the University of West Bohemia (UWB) and the thermochromic W-doped VO_2 layer using a controlled HiPIMS of a rotatable W-doped (1.5 at.%) V target at the Fraunhofer (FEP), see Table 1. Here, P_{av} is the deposition-averaged target power, P_{max} is the maximum target power in a pulse, t_{on} is the (negative) voltage pulse duration, f_r is the repetition frequency ($f_r = 1/T_p$ where T_p is the pulse period), t_{on}/T_p is the duty cycle, p_{ar} is the argon partial pressure, p_{ox} is the oxygen partial pressure, Φ_{ar} is the argon flow rate and Φ_{ox} is the oxygen flow rate.

Device	Target	P_{av} (kW)	P_{max} (kW)	t_{on} (μs)	f_r (Hz)	t_{on}/T_p (%)	p_{ar} (Pa)	p_{ox} (Pa)	Φ_{ar} (sccm)	Φ_{ox} (sccm)
UWB	V	0.27	27.49	80	625	5.00	1.00	0.02-0.05	60	1.45-1.85
	W	0.69×10^{-3}	16.02×10^{-3}	16	5000	8.00	1.00	0.02-0.05	60	1.45-1.85
FEP	V-W	6.00	276.45	70	750	5.25	0.20	0.00-0.02	250	0-50

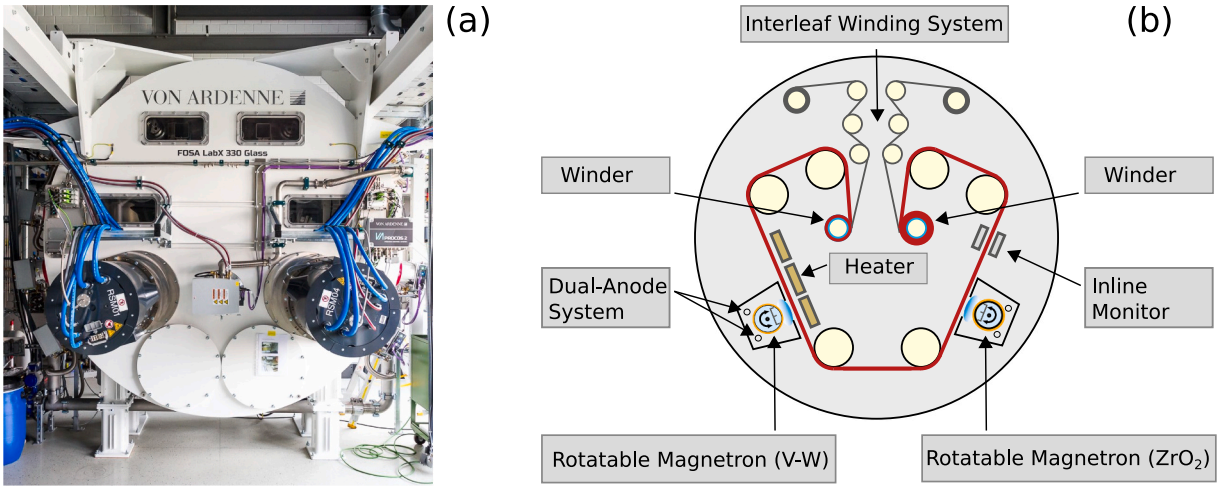

Fig. 1. (a) Photo and (b) schematic diagram of the large-scale roll-to-roll device used for depositions of ZrO_2/W-doped VO_2/ZrO_2 coatings at the Fraunhofer FEP (see Table 1).

minimize arcing on the sputtered targets and to avoid a "disappearing anode" effect. The pressures during the depositions were measured using two (one for each sputter chamber) capacitance manometers (Baratron, Type 627D, MKS).

The UFG substrate was guided between two winders. Both the bottom and the top ZrO_2 layer were deposited using the magnetron with the ZrO_2 target during the UFG substrate motion with a band speed of 0.15 m/min from the right-side winder to the left-side winder, as viewed from the front of the device. The W-doped VO_2 layer was deposited using the magnetron with the V-W target during the UFG substrate motion with a band speed of 0.10 m/min from the left-side winder to the right-side winder.

The W-doped VO_2 layer was deposited by controlled HiPIMS of the V-W target at a substrate surface temperature close to 350 °C. This T_s value was estimated on the basis of the evaluations presented for the same device recently [19]. The argon flow rate was 250 sccm corresponding to $p_{ar} = 0.20$ Pa, while the total Φ_{ox} in eight O_2 inlets, placed in front of and along the sputtered V-W target and oriented to the substrate, was 0 or 50 sccm (see Fig. 2 and Table 2). The moments of switching of the Φ_{ox} pulses from one value to the other were determined during the deposition by a programmable logic controller, developed at the UWB, which was adapted (modification of analog inputs and outputs, and optimization of the controller software interface) to the large-scale roll-to-roll device at the FEP. In contrast to the aforementioned deposition of the $V_{0.984}W_{0.016}O_2$ layer at the UWB [16], a pre-selected critical value of p_{ox} (as in [21,22]) determined switching of the Φ_{ox} during the depositions of the W-doped VO_2 layers with a fixed $p_{ar} = 0.20$ Pa at the FEP. When the increasing monitored p_{tot} reached the critical value $(p_{tot})_{cr} = 0.21$ Pa (marked by a dashed line in Fig. 2a), the process controller sent a signal to the input of the O_2 mass flow controller to switch off the oxygen flow $\Phi_{ox} = 50$ sccm. When the decreasing monitored p_{tot} reached the critical value $(p_{tot})_{cr} = 0.21$ Pa again, the process controller sent a signal to the O_2 mass flow controller to switch on the oxygen flow $\Phi_{ox} = 50$ sccm. Fig. 2a shows a delayed opening and fast closing of the O_2 mass flow controller. The magnetron with the V-W target was driven by a high-power pulsed dc power supply (20 kW HIPV, Ingeniería Viesca, S.L.). The voltage pulse duration was 70 μs at a repetition frequency of 750 Hz (duty cycle of 5.25%) and the deposition-averaged target power was 6 kW (see Table 2). The corresponding deposition-averaged target power density (spatially averaged over the total target area being sputtered at a given time) was approximately 10 Wcm^{-2}.

The basic principle of the used sputter technique is presented in Fig. 2, which shows the time evolution of the magnetron voltage, $U_d(t)$, and the target current, $I_d(t)$, during a deposition of the W-doped VO_2 layer. As can be seen in Fig. 2, the waveforms of $U_d(t)$ and $I_d(t)$ oscillate during the deposition in a dependence on the value of p_{ox} in the discharge, being in the range from 0 to 0.02 Pa (see Fig. 2a). The corresponding maximum target currents in a pulse were 470 A and 570 A, respectively, at almost the same magnetron voltage of 485 V (see Fig. 2b). The much higher values of $I_d(t)$ at the highest p_{ox}, leading to a maximum target power of 276 kW in a pulse, can be explained [22]: (i) by a significantly enlarged flux of the O_2^+ and O^+ ions, arising in front of the partly oxidized V-W target at an increased local oxygen partial pressure, and (ii) by an increased secondary-electron emission yield of the V-W target with a larger compound coverage, particularly for the impacting O_2^+ and O^+ ions.

The advantages of the used pulsed O_2 flow control are: (i) very high process stability (no problems with inertia of the inlet system, delay of valves and sensors, and hysteresis effects) as the controller does not try to keep one value but allows for a pre-selected interval of an output variable in accordance with the control-theory literature dealing with

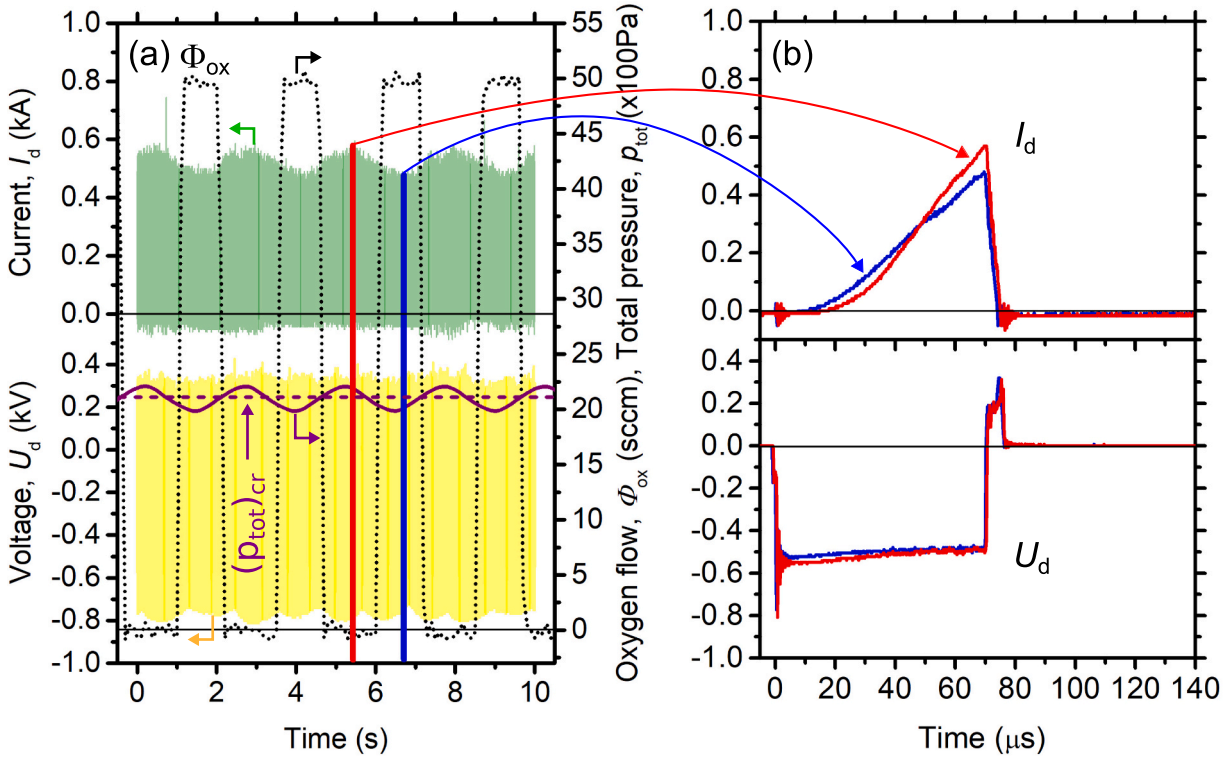

Fig. 2. (a) The contours of the shaded areas represent the magnetron voltage, U_d, and the target current, I_d, during a deposition of the W-doped VO_2 layer using the large-scale roll-to-roll device (Tables 1 and 2). A pre-selected critical value of the total pressure $(p_{tot})_{cr} = 0.21$ Pa determining the switching between the oxygen flow rate $\Phi_{ox} = 0$ and 50 sccm is marked by a dashed line. The Φ_{ox} values measured at the output from the O_2 mass flow controller are marked by dotted lines. (b) Time evolution of the U_d and I_d values at the rotatable V-W magnetron target during the pulses related to the minimum and maximum values of the oxygen partial pressure.

the control of non-linear systems [24], (ii) simplicity, as no additional measurement devices (such as a plasma emission monitoring system, mass spectrometer or Lambda sensor) are needed, and (iii) applicability to large-area industrial coaters as a multi-segment O_2 injection control can be used.

As can be seen in Fig. 2, short-lived high positive U_d overshoots (over 300 V) with the corresponding large electron fluxes drawn from the plasma onto the target (see the negative values of I_d) can be identified after the negative U_d pulses. These electron fluxes quickly neutralize the positive charge accumulated on non-conducting parts of the target surface during negative U_d pulses. As a consequence, the arcing on the target surface is minimized. The I_d oscillations appearing at the very beginning of the negative U_d pulses are oscillating capacity currents, accompanied by the voltage oscillations, in the power supply circuit caused by fast negative voltage transitions on the power supply.

Both the bottom and the top ZrO_2 layer were deposited by unipolar pulsed dc magnetron sputtering onto the substrate without an external heating. The total pressure was 0.40 Pa at $\Phi_{ar} = 250$ sccm and $\Phi_{ox} = 8$ sccm. The magnetron with the ZrO_2 target was driven by a dc power supply (Type 20 k, TLU GmbH) combined with a pulse unit (UBS-C2, Fraunhofer FEP). The voltage pulse duration was 16 μs at a repetition frequency of 50 kHz (duty cycle of 80%) and the deposition-averaged target power was 6 kW.

To support the crystallinity of the W-doped VO_2 layers and to improve the uniformity of the coatings, a post annealing of the three-layer ZrO_2/W-doped VO_2/ZrO_2 coatings was carried out at an estimated temperature close to 320 °C, when the coatings passed along the radiation heater near the sputter chamber with the V-W magnetron (see Fig. 1) after the deposition of the top ZrO_2 layer. The turn-on of this heater had only a slight effect on the T_s value during the deposition of the top ZrO_2 layer using the ZrO_2 magnetron.

2.2. Coating characterization

The thickness and room-temperature (23 °C) optical constants (refractive index, n, and extinction coefficient, k) of individual layers were measured by spectroscopic ellipsometry using the J.A. Woollam Co. Inc. VASE instrument. The precision was enhanced by dividing the analysis into two steps: (i) characterization of the bottom ZrO_2 layer without the rest of the coating (the top ZrO_2 layer was expected to have the same properties) and (ii) characterization of the whole coating, using the properties of ZrO_2 as input quantities. The measurements were performed at the angles of incidence of 55, 60 and 65° in reflection, in the wavelength (λ) range from 300 to 2000 nm. Below we give n and k at $\lambda = 550$ nm, n_{550} and k_{550}. The optical data were fitted using the WVASE software and an optical model which included the UFG substrate, ZrO_2 layers represented by the Cauchy oscillator, a W-doped VO_2 layer represented by a combination of the Cody-Lorentz oscillator with Lorentz oscillators and a surface roughness layer.

The coating transmittance, T, was measured at a temperature T_m between $T_{ms} = -10$ °C (semiconducting state well below T_{tr}) and $T_{mm} = 70$ °C (metallic state well above T_{tr}) using the Agilent CARY 7000 spectrophotometer equipped with an in-house made heat/cool stage. Below we present (i) T at $\lambda = 2500$ nm, T_{2500}, measured in the whole T_m range in order to evaluate T_{tr} and (ii) spectroscopic $T(\lambda)$ measured in the λ range from 300 to 2500 nm at the extremal temperatures T_{ms} and T_{mm} in order to evaluate the integral transmittances. The luminous transmittance was calculated as

$$T_{lum}(T_m) = \frac{\int_{380}^{780} \varphi_{lum}(\lambda)\varphi_{sol}(\lambda)T(T_m,\lambda)d\lambda}{\int_{380}^{780} \varphi_{lum}(\lambda)\varphi_{sol}(\lambda)d\lambda}, \quad (1)$$

where φ_{lum} is the luminous sensitivity of the human eye and φ_{sol} is the sea-level solar irradiance, the solar energy transmittance was calculated as

$$T_{sol}(T_m) = \frac{\int_{300}^{2500} \varphi_{sol}(\lambda) T(T_m, \lambda) d\lambda}{\int_{300}^{2500} \varphi_{sol}(\lambda) d\lambda} \quad (2)$$

and their modulations were calculated as

$$\Delta T_{lum} = T_{lum}(T_{ms}) - T_{lum}(T_{mm}), \quad (3)$$

$$\Delta T_{sol} = T_{sol}(T_{ms}) - T_{sol}(T_{mm}). \quad (4)$$

A homogeneous temperature field has been achieved by supporting the 0.1 mm thick UFG by an underlying 1 mm thick conventional soda-lime glass, at a cost of introducing a thin air layer over most of the contact area between both glass layers. Note that the additional interference at this air layer (not included in the optimized coating design which is described in Sec. 3.1 and which leads to an interference maximum of T_{lum}) decreases the measured T_{lum} by ≈4% according to experiments (shown in [16]) as well as optical modelling (not shown).

The coating color was calculated from the transmittance or similarly measured reflectance [16] for the CIE 1931 2° standard observer and the CIE daylight illuminant D65.

The cross-sectional micrograph of the broken and ion-polished multilayered coating prepared in the large-scale roll-to-roll device at the FEP was acquired by scanning electron microscopy (SEM) using the Hitachi SU-70 instrument (incident beam energy of 5 keV). The room-temperature (25 °C) crystal structure of the same coating was investigated by X-ray diffraction (XRD) using the PANalytical X'Pert PRO instrument working with a CuKα (40 kV, 40 mA) radiation at a glancing incidence of 1°.

The W content in the metal sublattice of the $V_{0.984}W_{0.016}O_2$, i.e. 1.6 ± 0.6 at.%, thermochromic (TC) layer prepared in the laboratory-scale device at the UWB was measured on a dedicated 290 nm thick layer (using the same substrate) in the aforementioned scanning electron microscope SU-70 using wave-dispersive spectroscopy (Magnaray, Thermo Scientific) at a primary electron energy of 7 keV.

3. Results and discussion

3.1. Coating design

While the coating design used has been explained and experimentally verified in the laboratory-scale device (UWB) previously [25], the cross-section SEM image shown in Fig. 3a confirms its successful realization in the large-scale roll-to-roll device (FEP). The roles of individual layers and their refractive indices obtained in the latter device are shown in Fig. 3b. As indicated by the formula ZrO_2/W-doped VO_2/ZrO_2, an important part of the coating design are ZrO_2 antireflection (AR) layers both below (thickness h_b) and above (thickness h_t) the TC layer (thickness h = 71 nm (UWB) or 69 nm (FEP)). The deposition protocol described in Sec. 2.1 led to well densified stoichiometric ZrO_2 characterized by n_{550} = 2.09 (UWB) or even 2.19 (FEP) and to W-doped VO_2 characterized by n_{550} = 2.82 (UWB) or n_{550} = 2.73 (FEP). The corresponding k_{550} values on the order of at most 10^{-3} (ZrO_2) and ≈0.4–0.5 (VO_2) are neglected in the considerations below. This makes n_{550} of the AR layers very close to the geometric mean of those of the TC layer and the glass (bottom AR layer) and sufficiently close to the geometric mean of those of the TC layer and the air (top AR layer), fulfilling the condition for AR layers shifting the upper envelope of the interference curve $T(\lambda)$ as close to 100% as possible. Further advantages of ZrO_2 include (i) easily achievable crystallinity (example in Fig. 4) at the deposition temperature used, which gives the bottom AR layer a second role of structure template improving the crystallinity of the TC layer [12,26], and (ii) high hardness (for an oxide), which gives the top AR layer a second role of a mechanical protection of the TC layer.

The maximization of T_{lum} requires not only as high upper envelope of $T(\lambda)$ as possible but also positioning of one of the interference maxima which touch this upper envelope close to λ = 550 nm. While the former is achieved by proper n_{550} of the AR layers, the latter is achieved by proper thickness of the AR layers. The first approximation can be given by treating each AR layer separately and once again neglecting k_{550}, leading to the well known formulas $h_{b,t} = \lambda/[4n_{550}]$ (quarter-wavelength layers), $3\lambda/[4n_{550}]$ (three-quarter wavelength layers), etc. Precise calculations (e.g. not neglecting k) of integral T_{lum} (shown in [25]) yield slightly different numbers, e.g. n_{550} = 2.15 leads to first-order maxima of T_{lum} around $h_{b,t}$ = 45 nm (less than 550/[4 × 2.15] = 64 nm) and second-order maxima of T_{lum} around $h_{b,t}$ = 180 nm (less than 3 × 550/[4 × 2.15] = 192 nm). The ideal $h_{b,t}$ values are almost independent of h, and they are approximately inversely proportional to n_{550} in order to fix the optical path length (180 × 2.15).

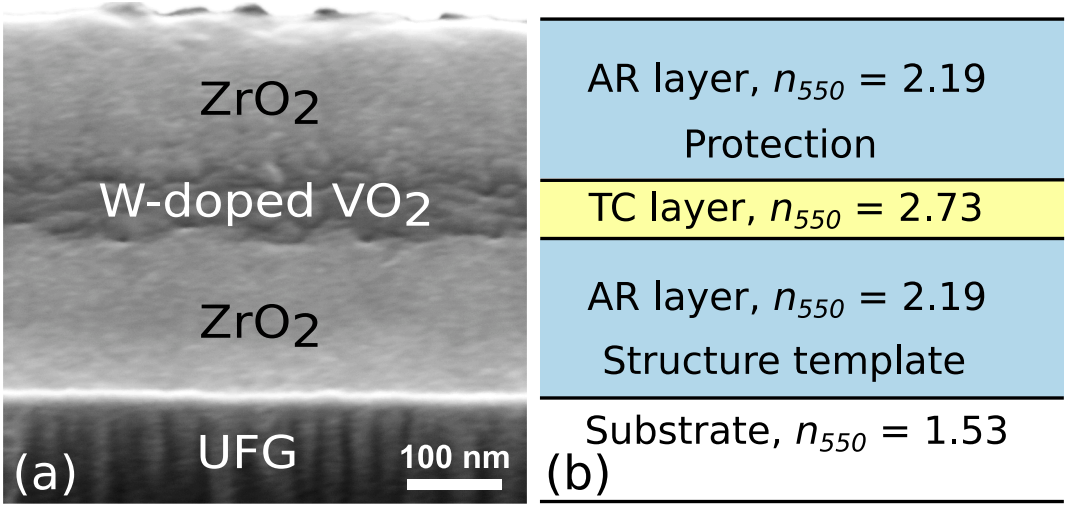

Fig. 3. (a) Cross-section SEM image of the ZrO_2/W-doped VO_2/ZrO_2 coating on ultrathin flexible glass (UFG) prepared using the large-scale roll-to-roll device. (b) Schematic diagram of the coating with characterization of the functions of the individual layers and their refractive indices at the wavelength of 550 nm, n_{550}, measured at T_m = 23 °C. Here, AR stands for the antireflection layers and TC stands for the thermochromic layer.

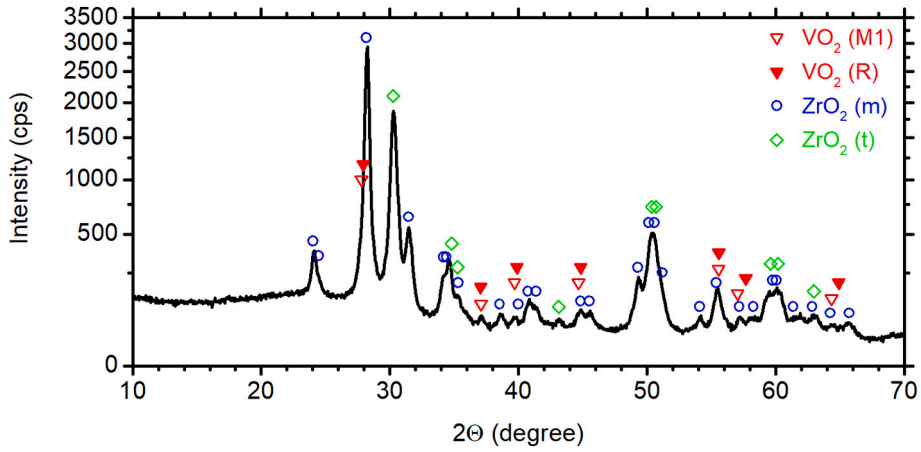

Fig. 4. X-ray diffraction patterns taken at T_m = 25 °C from the ZrO_2 (167 nm)/W-doped VO_2 (69 nm)/ZrO_2 (167 nm) coating on ultrathin flexible glass prepared using the large-scale roll-to-roll device. The main diffraction peaks of VO_2 (R), VO_2 (M1), ZrO_2 (m) and ZrO_2 (t) are marked.

Next, it is necessary to consider that the criterion of success is simultaneous optimization of T_{lum} and ΔT_{sol}. On the one hand, the first-order maximum of $T(\lambda)$ in the visible does not lead to anything special in the infrared where most of the energy saving is required to take place. Consequently, the first-order AR layers lead to high T_{lum} but relatively low ΔT_{sol}. On the other hand, the second-order maximum of $T(\lambda)$ in the visible leads to a first-order maximum of $T(\lambda)$ in the infrared (example in Fig. 5), increasing the potential for T modulation in this λ range. Consequently, the second-order AR layers lead to about the same T_{lum} as the first-order AR layers but to a much higher ΔT_{sol} [25]. Indeed, the thicknesses of the AR layers deposited, h_b = 172 nm and h_t = 178 nm (UWB) or $h_b = h_t$ = 167 nm (FEP), almost exactly lead to second-order maxima of T_{lum}: [180 × 2.15]/[(172 or 178) × 2.09] = 104 or 108% (UWB) and [180 × 2.15]/[167 × 2.19] = 106% (FEP). Note that the total thickness of the latter coating as measured by spectroscopic ellipsometry, $h_b + h + h_t$ = 167 + 69 + 167 = 403 nm, very well corresponds to the cross-section SEM image in Fig. 3a. Following the design even more precisely is desired for industrial production, but beyond the aim to demonstrate the transferability to the large-scale device in itself.

3.2. Coating structure and properties

The XRD pattern of the coating prepared in the large-scale roll-to-roll device (FEP) is shown in Fig. 4. First and most importantly, the figure shows that the only crystalline phases identified in the TC layer are the desired thermochromic polymorphs VO_2(M1) (PDF#04-003-2035 [27]) and VO_2(R) (PDF#01-073-2362). There is not any contribution of metastable non-thermochromic polymorphs such as VO_2(B) or VO_2(P), and there is not any contribution of non-thermochromic phases with slightly different stoichiometries such as V_9O_{17} or V_6O_{13} (let alone V_2O_5, the thermodynamically preferred phase under O-rich conditions).

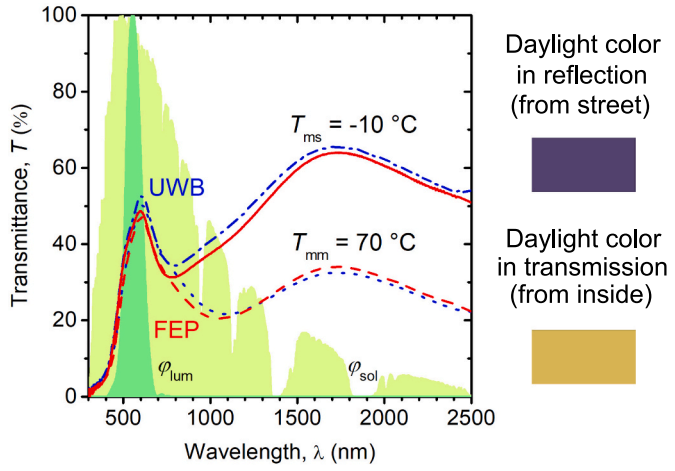

Fig. 5. The transmittance as a function of the wavelength for the ZrO_2 (167 nm)/W-doped VO_2 (69 nm)/ZrO_2 (167 nm) coating prepared using the large-scale roll-to-roll device (FEP, solid and dashed line) and for the ZrO_2 (172 nm)/$V_{0.984}W_{0.016}O_2$ (71 nm)/ZrO_2 (178 nm) coating prepared using the laboratory-scale device (UWB, dash-dotted and dotted line). During the measurements at the temperatures T_{ms} = −10 °C (significantly below T_{tr}) and T_{mm} = 70 °C (significantly above T_{tr}), the samples on ultrathin glass were supported by an underlying 1 mm thick soda-lime glass. The contours of the shaded areas represent the luminous sensitivity of the human eye (φ_{lum}) and the sea-level solar irradiance spectrum at an air mass of 1.5 (φ_{sol}), normalized to maxima of 100%. The daylight colors in transmission and reflection calculated for the UWB coating are presented.

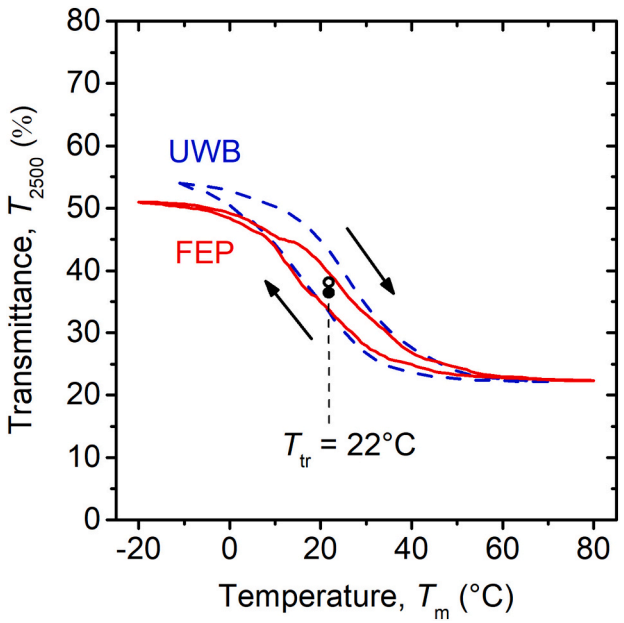

Fig. 6. Temperature (T_m) dependence of the transmittance T_{2500} at 2500 nm for the ZrO_2 (167 nm)/W-doped VO_2 (69 nm)/ZrO_2 (167 nm) coating prepared using the large-scale roll-to-roll device (FEP) and the ZrO_2 (172 nm)/$V_{0.984}W_{0.016}O_2$ (71 nm)/ZrO_2 (178 nm) coating prepared using the laboratory-scale device (UWB), see Fig. 5. The transition temperature T_{tr} = 22 °C is marked.

Table 3
Thermochromic properties of the ZrO_2 (167 nm)/W-doped VO_2 (69 nm)/ZrO_2 (167 nm) coating and the ZrO_2 (172 nm)/$V_{0.984}W_{0.016}O_2$ (71 nm)/ZrO_2 (178 nm) coating deposited on ultrathin flexible glass (UFG) using the large-scale roll-to-roll device (FEP) and the laboratory-scale device (UWB), respectively. The measured T values are underestimated by ≈ 4% owing to the effect of the very thin air layer arising between the UFG substrate and an underlying supporting 1 mm thick soda-lime glass used during the measurements (see Section 2.2).

Device	T_{lum} (T_{ms})	T_{lum} (T_{mm})	ΔT_{lum}	T_{sol} (T_{ms})	T_{sol} (T_{mm})	ΔT_{sol}
	(%)	(%)	(%)	(%)	(%)	(%)
FEP	43.2	40.5	2.7	37.0	28.3	8.7
UWB	45.7	42.2	3.5	39.6	30.0	9.6

Second, the simultaneous presence of VO_2(M1) and VO_2(R) strongly indicates that the doping by W has been successful and that the transition temperature is close to room temperature at which the measurement took place (see Fig. 6 for more details). Third, the figure confirms that the AR layers are well crystalline, see the strong narrow peaks corresponding to monoclinic ZrO_2 (ZrO_2(m); PDF#04-013-6875) with a contribution of tetragonal ZrO_2 (PDF#01-081-1544 valid for $ZrO_{1.95}$). This supports the aforementioned second role of the bottom AR layer (structure template which improves the crystallinity of the TC layer).

The success of the transfer from the laboratory-scale device (UWB) to the large-scale roll-to-roll device (FEP) is quantified by comparison of the performance of both multilayered coatings in terms of spectroscopic $T(\lambda)$ in Fig. 5, integral quantities calculated using $T(\lambda)$ in Table 3 and T_{tr} in Fig. 6. All interference curves $T(\lambda)$ shown in Fig. 5 are characteristic of the design explained in Sec. 3.1: see the first-order maximum of $T(\lambda)$ in the infrared and the second-order maximum of $T(\lambda)$ in the visible. The strongly temperature-dependent maximum of $T(\lambda)$ in the infrared is largely responsible for the relatively high ΔT_{sol} approaching 10% as shown in Table 3. The almost temperature-independent maximum of $T(\lambda)$ in the visible is responsible for the relatively high T_{lum} of 45–50% as also shown in Table 3, taking into account (Sec. 2.2) that the T_{lum} values in Table 3 are by ≈4% lower than the T_{lum} values which truly characterize the coatings but which could not be directly measured because of the thin air layer between the UFG substrate and the underlying supporting glass. The temperature independence of T_{lum} (ΔT_{lum} shown in Table 3 of only ≈3%) constitutes an important advantage of the presented coatings over other solutions where the energy saving takes place primarily in the visible. The complicated dispersion of optical constants leads to a yellowish color in transmission and bluish color in reflection (visualized in Fig. 5; the fact that the coating color is almost independent of the temperature is presented in detail in [16]).

Most importantly, it can be seen that the transfer to the large-scale device led not only to qualitatively the same multilayered structure (Fig. 3) and crystal structure (Fig. 4), but also to quantitatively almost the same properties. Fig. 5 shows that the interference curves $T(\lambda)$ exhibited by both coatings are very similar, both horizontally (in agreement with similar optical path lengths in AR layers given in Sec. 3.1) and vertically (in agreement with similar h values of 69–71 nm). A case can be made that the FEP coating exhibits not only ΔT_{sol} by ≈1% lower (which is consistent with slightly lower h) but also $T(\lambda)$ in the visible and in turn T_{lum} by ≈2% lower (which is contrary to slightly lower h). However, these small differences are within the usual dependence of k_{550} of VO_2 on the exact deposition conditions and on the probable consequent tiny changes in the O content (an important open question in this field, beyond the scope of the present paper). In parallel, Fig. 6 shows that the doping of VO_2 by W has been equally successful in both cases, leading to the same T_{tr} (as defined by a half of the total T_{2500} change, averaged over both branches of the hysteresis loop) of 22 °C. The occasionally reported harmful effect of W on the thermochromic performance of VO_2 prepared using e.g. the sol-gel method [28] or the hydrothermal synthesis [29] has not been observed using any of the two presented deposition protocols based on the controlled reactive HiPIMS.

4. Conclusions

There is only one sputter technique of VO_2-based thermochromic coatings for energy-saving smart windows which previously led to a combination of all the key achievements at least on the laboratory scale: low surface temperature (330 °C) of conventional glass or flexible glass substrates without any substrate bias voltage and post-deposition annealing, and low thermochromic transition temperature down to ≈20 °C at a competitive luminous transmittance and modulation of the solar energy transmittance [16]. We have carried out a successful transfer of this technique based on controlled reactive HiPIMS to a large-scale (300 mm × 20 m substrates) roll-to-roll deposition device. Using the same ultrathin flexible glass substrate and almost the same substrate temperature (close to 350 °C), we have used this large-scale device to prepare qualitatively the same ZrO_2/W-doped VO_2/ZrO_2 coating which has been prepared previously on the laboratory scale, including (i) the desired crystal structure of individual layers, (ii) almost the same optical path lengths in the second-order ZrO_2 antireflection layers and (iii) a tungsten doping level leading to exactly the same thermochromic transition temperature.

We have confirmed that the coating consequently exhibits almost the same values of luminous transmittance and modulation of the solar energy transmittance. The results constitute an important step toward industrialization of coatings prepared by controlled reactive HiPIMS in general and of energy-saving thermochromic coatings in particular.

CRediT authorship contribution statement

Jiří Rezek: Investigation, Data curation, Visualization. **Jolanta Szelwicka**: Investigation, Data curation. **Jaroslav Vlček**: Conceptualization, Methodology, Writing - original draft, Writing - review & editing. **Radomír Čerstvý**: Investigation. **Jiří Houška**: Writing – original draft. **Matthias Fahland**: Conceptualization. **John Fahlteich**: Conceptualization.

Declaration of competing interest

The authors declare that they have no known competing financial interests or personal relationships that could have appeared to influence the work reported in this paper.

Acknowledgments

This research was funded from The European Union's Horizon 2020 Research and Innovation Programme under Grant Agreement No. 869929, Project “Switch2Save”.

References

[1] F.J. Morin, Oxides which show a metal-to-insulator transition at the Neel temperature, Phys. Rev. Lett. 3 (1959) 34–36.
[2] H.A. Wriedt, The O-V (oxygen-vanadium) system, Bull. Alloy Phase Diagr. 10 (1989) 271–277.
[3] Y. Ke, S. Wang, G. Liu, M. Li, T.J. White, Y. Long, Vanadium dioxide: the multistimuli responsive material and its applications, Small 14 (2018) 1802025.
[4] K. Liu, S. Lee, S. Yang, O. Delaire, J. Wu, Recent progresses on physics and applications of vanadium dioxide, Mater. Today 21 (2018) 875–896.
[5] R. Shi, N. Shen, J. Wang, W. Wang, A. Amini, N. Wang, C. Cheng, Recent advances in fabrication strategies, phase transition modulation, and advanced applications of vanadium dioxide, Appl. Phys. Rev. 6 (2019), 011312.
[6] C.G. Granqvist, Recent progress in thermochromics and electrochromics: a brief survey, Thin Solid Films 614 (2016) 90–96.
[7] Y. Gao, H. Luo, Z. Zhang, L. Kang, Z. Chen, J. Du, M. Kanehira, C. Cao, Nanoceramic VO_2 thermochromic smart glass: a review on progress in solution processing, Nano Energy 1 (2012) 221–246.
[8] S. Wang, M. Liu, L. Kong, Y. Long, X. Jiang, A. Yu, Recent progress in VO_2 smart coatings: strategies to improve the thermochromic properties, Prog. Mater. Sci. 81 (2016) 1–54.
[9] M. Li, S. Magdassi, Y. Gao, Y. Long, Hydrothermal synthesis of VO_2 polymorphs: advantages, challenges and prospects for the application of energy efficient smart windows, Small 13 (2017) 1701147.

[10] F. Xu, X. Cao, H. Luo, P. Jin, Recent advances in VO_2-based thermochromic composites for smart windows, J. Mater. Chem. C 6 (2018) 1903–1919.
[11] T.-C. Chang, X. Cao, S.-H. Bao, S.-D. Ji, H.-J. Luo, P. Jin, Review on thermochromic vanadium dioxide based smart coatings: from lab to commercial application, Adv. Manuf. 6 (2018) 1–19.
[12] D. Kolenatý, J. Vlček, T. Bárta, J. Rezek, J. Houška, S. Haviar, High-performance thermochromic VO_2-based coatings with a low transition temperature deposited on glass by a scalable technique, Sci. Rep. 10 (2020) 11107.
[13] G. Sun, X. Cao, X. Li, S. Bao, N. Li, M. Liang, A. Gloter, H. Gu, P. Jin, Low-temperature deposition of VO_2 films with high crystalline degree by embedding multilayered structure, Sol. Energy Mater. Sol. Cells 161 (2017) 70–76.
[14] T. Chang, X. Cao, N. Li, S. Long, X. Gao, L.R. Dedon, G. Sun, H. Luo, P. Jin, Facile and low-temperature fabrication of thermochromic Cr_2O_3/VO_2 smart coatings: enhanced solar modulation ability, high luminous transmittance and UV-shielding function, ACS Appl. Mater. Interfaces 9 (2017) 26029–26037.
[15] J.-P. Fortier, B. Baloukas, O. Zabeida, J.E. Klemberg-Sapieha, L. Martinu, Thermochromic VO_2 thin films deposited by HiPIMS, Sol. Energy Mater. Sol. Cells 125 (2014) 291–296.
[16] T. Bárta, J. Vlček, J. Houška, S. Haviar, R. Čerstvý, J. Szelwicka, M. Fahland, J. Fahlteich, Pulsed magnetron sputtering of strongly thermochromic VO_2-based coatings with a transition temperature of 22 °C onto ultrathin flexible glass, Coatings 10 (2020) 1258.
[17] M. Junghähnel, J. Westphalen, Processing on flexible glass-challenges and opportunities, SVC Bull. Fall/Winter (2017) 31–39.
[18] M. Junghähnel, J. Fahlteich, Thin-film deposition on flexible glass by plasma processes, in: S.M. Garner (Ed.), Flexible Glass: Enabling Thin, Lightweight, and Flexible Electronics, 1st ed., Scrivener Publishing LLC, Beverly, CA, USA, 2017, pp. 129–180.
[19] M. Fahland, O. Zywitzki, T. Modes, K. Vondkar, T. Werner, C. Ottermann, M. Berendt, G. Pollack, Roll-to-roll sputtering of indium tin oxide layers onto ultrathin flexible glass, Thin Solid Films 669 (2019) 56–59.
[20] L. Dai, S. Chen, J. Liu, Y. Gao, J. Zhou, Z. Chen, C. Cao, H. Luo, M. Kanehira, F-doped VO_2 nanoparticles for thermochromic energy-saving foils with modified color and enhanced solar-heat shielding ability, Phys. Chem. Chem. Phys. 15 (2013) 11723–11729.
[21] J. Vlček, D. Kolenatý, J. Houška, T. Kozák, R. Čerstvý, Controlled reactive HiPIMS - effective technique for low-temperature (300 °C) synthesis of VO_2 films with semiconductor-to-metal transition, J. Phys. D. Appl. Phys. 50 (2017) 38LT01.
[22] J. Vlček, D. Kolenatý, T. Kozák, J. Houška, J. Čapek, Š. Kos, Ion-flux characteristics during low-temperature (300 °C) deposition of thermochromic VO_2 films using controlled reactive HiPIMS, J. Phys. D. Appl. Phys. 52 (2019), 025205.
[23] W.D. Sproul, D.J. Christie, D.C. Carter, Control of reactive sputtering processes, Thin Solid Films 491 (2005) 1–17.
[24] J. Bechhoefer, Feedback for physicists: a tutorial essay on control, Rev. Mod. Phys. 77 (2005) 783–836.
[25] J. Houska, D. Kolenaty, J. Vlcek, T. Barta, J. Rezek, R. Cerstvy, Significant improvement of the performance of $ZrO_2/V_{1-x}W_xO_2/ZrO_2$ thermochromic coatings by utilizing a second-order interference, Sol. Energy Mater. Sol. Cells 191 (2019) 365–371.
[26] J.C. Jiang, T. Bárta, J. Vlček, J. Houška, E.I. Meletis, Microstructure of high-performance thermochromic $ZrO_2/V_{0.984}W_{0.016}O_2/ZrO_2$ coating with a low transition temperature (22 °C) prepared on flexible glass, Surf. Coat. Technol. 424 (2021), 127654.
[27] The International Centre for Diffraction Data, PDF-4+ Database; the International Centre for Diffraction Data: Newtown Square, PA, USA, 2015.
[28] L. Hu, H. Tao, G. Chen, R. Pan, M. Wan, D. Xiong, X. Zhao, Porous W-doped VO_2 films with simultaneously enhanced visible transparency and thermochromic properties, J. Sol-Gel Sci. Technol. 77 (2016) 85–93.
[29] N. Shen, S. Chen, Z. Chen, X. Liu, C. Cao, B. Dong, H. Luo, J. Liu, Y. Gao, The synthesis and performance of Zr-doped and W–Zr-codoped VO_2 nanoparticles and derived flexible foils, J. Mater. Chem. A2 (2014) 15087–15093.